Chinese Chemical Letters 35 (2024) 109835

Contents lists available at ScienceDirect

Chinese Chemical Letters

journal homepage: www.elsevier.com/locate/cclet

Facile preparation of ZIF-8/ZIF-67-derived biomass carbon composites for highly efficient electromagnetic wave absorption

Xuexia Lin[a,*], Yihui Zhou[a,b], Jiafu Hong[a,c], Xiaofeng Wei[c], Bin Liu[c], Chong-Chen Wang[b,*]

[a] College of Chemical Engineering, Huaqiao University, Xiamen 361021, China
[b] Beijing Key Laboratory of Functional Materials for Building Structure and Environment Remediation, Beijing University of Civil Engineering and Architecture, Beijing 100044, China
[c] College of Materials Science and Engineering, Huaqiao University, Xiamen 361021, China

ARTICLE INFO

Article history:
Received 2 December 2023
Revised 28 February 2024
Accepted 25 March 2024
Available online 26 March 2024

Keywords:
Biomass
Metal organic framework
EMW absorption
Dielectric loss
Magnetic loss

ABSTRACT

Biomass absorbing materials have received increasing attention for electromagnetic wave (EMW) absorption field absorbing materials due to its low density and high dielectric loss. However, the biomass EMW absorbing materials often suffer from the insufficient magnetic loss and impedance matching. In this work, a facile ZIF-8/ZIF-67-derived biomass composites (CoZnO@BPC) was prepared for high-performance EMW absorption based on multi-component micro, nano structures metal particles and xanthoce sorbifolia bunge shells-derived biomass porous carbon (BPC). The dielectric loss and/or magnetic loss abilities of CoZnO@BPC composites were adjusted by changing the mass ratio of Zn^{2+} to Co^{2+} ions. Under the filled amount of 20 wt%, CoZnO@BPC exhibited excellent EMW absorption with the minimum reflection loss (RL) at 15.84 GHz is -50.2 dB, and the matching thickness is only 1.7 mm. By adjusting the ZIFs mass ratio, the effective absorption bandwidth (EAB) can be up to 5.92 GHz (from 12.08 GHz to 18 GHz), and the matching thickness is only 1.9 mm. The results provide a new insight for the economical and efficient preparation of lightweight and advanced microwave absorbing materials.

The booming electronic equipment provides a great opportunity to promote social development and meet the needs of the public, but a series of electromagnetic problems such as electromagnetic interference, electromagnetic pollution and electromagnetic leakage are inevitable. Faced with the rapid growth of serious electromagnetic pollution, the society urgently needs advanced electromagnetic wave (EMW) absorption materials with lightweight, wide and strong absorption. Biomass carbon has aroused great interest for the remarkable advantages of EMW absorption in weight reduction and high dielectric loss, as it possesses the abundant pore structures, large specific surface area, rich functional group, unique layered structure [1–3]. Besides, according to statistics, in addition to the normal daily needs of food and clothing, biomass waste or by-products account for half of the global waste. Therefore, the use of waste biomass can be considered as an effective strategy for reducing environmental pollution and the achievement of resource regeneration and utilization. However, biomass carbon has serious problems of insufficient magnetic loss and impedance mismatch, finally limits its further application in the field of EMW absorption [4–6]. Therefore, it requires the development of the multifunctional biomass materials to achieve the preferable absorption of EMW.

In order to improve impedance matching, the biomass-based composites were often made up with the multi-components for the achievement of remarkable dielectric loss and magnetic loss abilities. Some studies have found an effective and simple strategy that is the doping of metal-organic framework (MOF) [7,8]. Generally, biomass porous carbon (BPC) materials are obtained by pyrolysis, etching of MOF precursors, and the microstructure of BPC materials is the confines of MOF precursor [9]. Ji *et al.* selected wheat flour, rice and cotton biomass to prepare NPC and NPC/magnetic composites to eliminate electromagnetic radiation [10]. Che *et al.* carbonized waxberry make full use of its hierarchical structure to obtain high impedance matching and ultra-wide microwave absorption frequency [11]. Wu *et al.* loaded Co_3O_4 particles into reduced graphene oxide (rGO) and celery stalks derived carbon (CDC) to prepared Co_3O_4@(rGO)/CDC composite [12]. The dielectric and impedance matching properties of the composites can be adjusted by changing the mass ratio of rGO to CDC. Another method is to construct pore structures of BPC. Zhihui Zeng group prepared abundant hierarchical pores of pine needle-derived carbons for

* Corresponding authors.
E-mail addresses: linxuexia@hqu.edu.cn (X. Lin), wangchongchen@bucea.edu.cn (C.-C. Wang).

https://doi.org/10.1016/j.cclet.2024.109835
1001-8417/

microwave absorption and controllable electrical properties [13]. Xuefeng Yao and his co-workers conducted an in-depth analysis of the influence of pore structure on microwave absorption, which found that honeycomb height and grading honeycomb have greatly influence on microwave absorption [14]. As a result, rationally designed MOFs-derived BPC composites can regulate dielectric loss and/or magnetic loss abilities, finally induce the impedance matching. Therefore, it was hypothesized that multiple MOFs could adjust dielectric loss and/or magnetic loss abilities because of the induce of different metal ion and that BPCs could modify as for preferable EMW-absorbing materials.

To test the hypothesis, ZIF-8 and ZIF-67 were used. These two MOFs materials have been well-studied and decorated to carbon materials. They were used to modulate the dielectric permittivity and magnetic permeability of composites through component changes, which would further adjust the impedance matching. Moreover, the EMW absorbing capacities would be improved due to the synergism of dielectric and magnetic loss mechanisms [15]. To verify the concept, waste Xanthoce Sorbifolia Bunge Shells (XSBS) were used to prepare BPC because XS are widely distributed in the northern and northeastern areas of China, and the amount of discarded XSBS reach hundreds of thousands of tons per year. The ZIF-8 and ZIF-67 were incorporated into BPC to form ZIF-8/ZIF-67-derived BPC (CoZnO@BPC). The composites were prepared by a simple carbonization process to control the magnetic loss of ZIF-8/ZIF-67. The effects of the mass ratio of Zn to Co and the filling ratio of the composite material to the paraffin matrix on the EMW absorption properties were investigated. The prepared composites were validated in terms of microstructure, impedance matching, and electromagnetic properties. Thus, the simple and effective strategy is developed for the preparation of high-performance EMW absorbents that will be promising in the field of electromagnetic pollution.

Biomass XSBS has a natural porous structure in the micron scale, which is an ideal raw material for making low-coated lightweight EMW carbon absorbing materials. At the same time, ZIF-8 and ZIF-67, as zeolite imidazole salt skeletons containing Zn/Co, have high porosity and are very suitable for direct pyrolysis of *in-situ* growth carbon materials to produce light porous metal particles [16]. By *in-situ* growth of ZIF-8/ZIF-67 particles on the surface of porous carbon biomass, a composite material contained Zn/Co particles prepared in Scheme 1.

The microstructure of CoZnO@BPC composites was characterized. As shown in Figs. 1a-f, the material presents a three-dimensional interconnecting porous carbon skeleton structure with rich pores and the size of each pore is about 1 μm. When MOFs were loaded to biomass XSBS and pyrolyzed, metal particles or metal oxides will be generated on the surfaces and pores of BPCs.

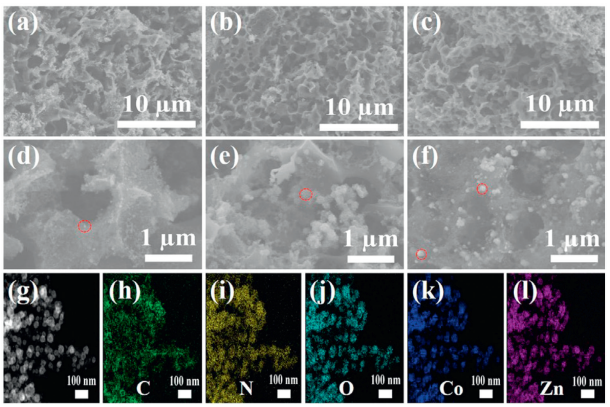

Fig. 1. SEM images of composites (a, d) CoZnO@BPC-11, (b, e) CoZnO@BPC-12, (c, f) CoZnO@BPC-21. (g-l) EDS element spectrogram of CoZnO@BPC-11.

The rich pores reduced the agglomeration of MOFs, promoted the dispersion of magnetic particles, and helped to improve the conduction and magnetic losses of ZIF derivatives. The EDS distributions of CoZnO@BPC-11 composites were analyzed by high angle annular dark field field-scanning TEM (FEI-TALOS-F200, Thermofisher Scientific). As shown in Figs. 1g-l, CoZnO@BPC-11 composite contains C, N, O, Co and Zn elements. Co and Zn nanoparticles were evenly dispersed in the material without serious caking. The heterogeneous interface formed between biomass carbon and metal nanoparticles has a high interface polarization ability, which is beneficial for EMW attenuation.

The morphology of the prepared CoZnO@BPC-11 composites were characterized by FE-SEM (field emission scanning electron microscope, SU5000, Hitachi), and HRTEM (high-resolution transmission electron microscope, FEI-TALOS-F200, Thermofisher Scientific) in Fig. 2. It can be seen that metal particles with an average grain size of about 20 nm are scattered on the surface of CoZnO@BPC-11 (Fig. 2a). In addition, tube fibers can be clearly seen around the nanoparticles (Figs. 2b and c). HRTEM in Figs. 2d and e show the lattice spacing of the composite material, and the strip spacing of the crystal faces is about 0.18 nm and 0.20 nm, corresponding to the (200) and (111) crystal faces of the Co nanoparticles [17]. The spacing between the crystal faces around the particles is about 0.25 nm and 0.28 nm, which is completely consistent with the (101) and (100) crystal faces of ZnO [18]. The crystal properties are also confirmed by the SAED diffraction pattern of electrons in the selected region (Fig. 2f). The SAED diagram shows that the main diffraction ring corresponds to (100) and (101) faces of ZnO and (111) and (200) faces of Co.

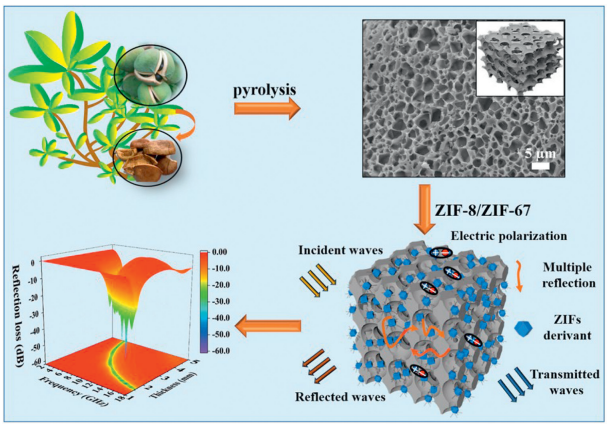

Scheme 1. Preparation process of CoZnO@BPC composites.

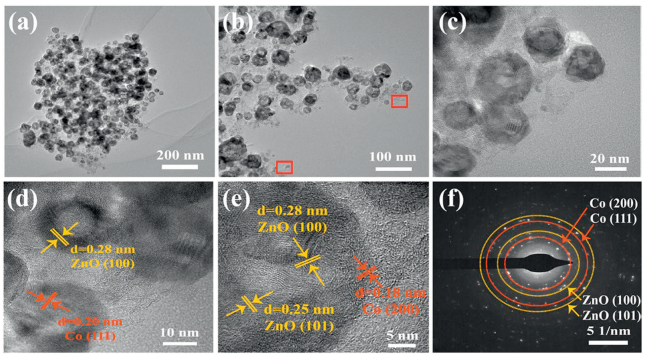

Fig. 2. CoZn@BPC-11 composite material (a, b) TEM image, (c-e) HRTEM image and (f) electron diffraction SEAD image.

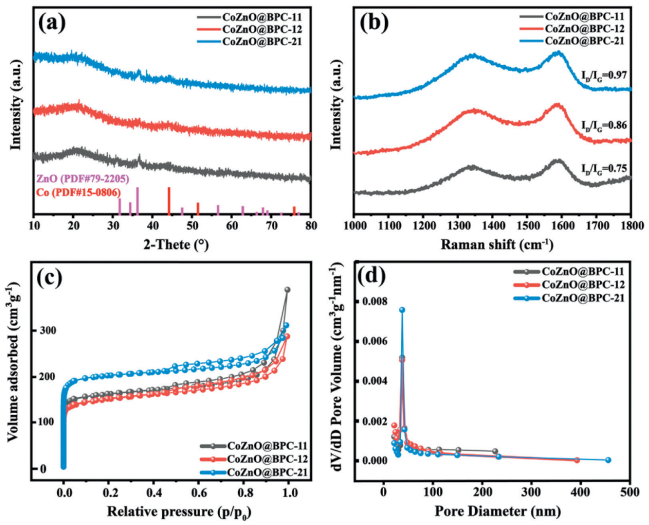

Fig. 3. CoZnO@BPC composite (a) XRD diffraction patterns, (b) Raman spectra, (c) N_2 adsorption-desorption curves, (d) pore size distribution diagram.

In order to further investigate the crystal structures and state properties of the prepared composites, the composites were analyzed and characterized by wide-angle XRD (Rigaku Smart Lab). As shown in Fig. 3a, all samples show broad diffraction peaks at 22.7°, corresponding to activated carbon. The existence of a wide diffraction peak indicates that the sample has amorphous characteristics and is an amorphous structural carbon. The three peaks at 44.2°, 51.5°, and 75.8° belong to the (111), (200), and (220) crystal faces of the metal Co, respectively (PDF #15-0806) [19]. In addition, the peaks at 31.8°, 34.4° and 36.3° belong to the (100), (001) and (101) crystal faces of the metal oxide ZnO (PDF #79-2205), respectively [20]. The degree of graphitization was analyzed by Raman spectroscopy. There are obvious characteristic peaks near 1345 cm^{-1} (D band) and 1575 cm^{-1} (G band), where the D band is corresponded to disordered or defective sp^3 hybrid carbon atoms, and the G band is corresponded to disordered or defective sp^2 hybrid carbon atoms in Fig. 3b. The intensity ratio of the two peaks (I_D/I_G) represents the degree of graphitization. The I_D/I_G ratios of CoZnO@BPC-11, CoZnO@BPC-12 and CoZnO@BPC-21 are 0.75, 0.86 and 0.97, respectively. This result indicates that CoZnO@BPC-11 has a small I_D/I_G ratio and a high degree of graphitization, which may be due to transition metal (Co) catalysis [21]. The increase of ZIF-8 ratio reduces the conversion of graphitic carbon during sintering. In addition, the high degree of graphitization of CoZnO@BPC-11 composites further improve the conductive loss capacity and help to improve the EMW dissipation capacity.

The valence states of CoZnO@BPC-11 composites were also analyzed by X-ray Photoelectron Spectroscopy (XPS, Nexsa, Thermofisher Scientific). The XPS full spectrum indicates that CoZnO@BPC-11 sample contains C, O, N, Co and Zn elements, the contents of which are 59.8 wt%, 6.1 wt%, 11.0 wt%, 3.1 wt% and 1.4 wt% respectively in Fig. S1 (Supporting information). Zn 2p can be divided into two peaks, Zn $2p_{3/2}$ at 1021.7 eV and Zn $2p_{1/2}$ at 1044.8 eV [22]. The Co 2p spectrum has six peaks. 781.1 eV corresponds to Co $2p_{3/2}$ and 796.5 eV to Co $2p_{1/2}$, 787.1 eV and 802.9 eV correspond to Co satellite peaks, and 779.6 eV and 794.7 eV correspond to Co [23]. The C 1s of the compositions can be divided into three peaks, which are 284.7 eV, 285.7 eV and 289.5 eV corresponding to C-C/C=C, C-O/C-N and O-C=O. The N 1s spectrum can be divided into three peaks, including pyridine nitrogen, pyrrole nitrogen and graphite nitrogen, which are 398.9 eV, 400.6 eV and 401.2 eV, respectively [24]. The O 1s is broken down into three peaks. Among them, the O-C bond is at 533.1 eV, and the binding energy of O=C is at 531.5 eV [25]. In addition, a characteristic peak of oxygen appears at 529.9 eV [26]. It can be seen from the XPS data that ZIFs has been successfully compounded onto BPC.

The N_2 adsorption-desorption curve and the magnetic hysteresis loops of CoZnO@BPC composites are studied. The samples present a type IV isotherm, when the relative pressure is low, the adsorption is rapid and obvious, then the adsorption remains unchanged, and when the relative pressure is increased, the adsorption is rapid. As shown in Fig. 3c, the specific surface areas of CoZnO@BPC-11, CoZnO@BPC-12 and CoZnO@BPC-21 are 635.17, 580.25 and 804.35 m^2/g, respectively. This was deduced that difference in the specific surface areas are due to the different mass ratio of ZIF-8 to ZIF-67. The average pore diameter of all samples is about 48 nm in Fig. 3d. The larger surface area of the composites can enhance the interaction between EMW and the hole wall, increase the transmission path and facilitate the multiple reflection and scattering of EMW. The magnetic properties of CoZnO@BPC at room temperature are measured by vibrating sample magnetometer (VSM). Saturation magnetization strength (Ms) and coercivity (Hc) are two important factors for magnetic loss ability. During the magnetization relaxation process, the larger magnetization capacity lead to the larger magnetic loss. CoZnO@BPC-21 shows higher the Ms and Hc values of 5.9 emu/g and 63.5 Oe, suggesting CoZnO@BPC-21 has a stronger magnetic loss capability in Fig. S2 (Supporting information).

The complex permittivity ($\varepsilon_r = \varepsilon' - j\varepsilon''$) and complex permeability ($\mu_r = \mu' - j\mu''$) are often used to evaluate EMW absorption performance. The storage capacity of electrical and magnetic energy is corresponded to ε' and μ', the dissipation capacity of the composites is corresponded to ε'' and μ''. The dielectric loss and magnetic loss capacity are thus characterized by the ratio of the complex permittivity ($tan\delta_e = {}^{\varepsilon''}/_{\varepsilon'}$) and the complex permeability ($tan\delta_m = {}^{\mu''}/_{\mu'}$) [27].

The frequency dependence of complex permittivity and permeability for the prepared CoZnO@BPC samples were recorded in 2-18 GHz under applied fields up to 10 kOe. As shown in Figs. 4a-c, the ε' values of the CoZnO@BPC composites decrease significantly over the entire frequency range. In contrast, CoZnO@BPC-21 decreases more, with the ε' value decreasing from 11.41 to 4.41. The ε" values of CoZnO@BPC composites show a decreasing and then increasing trend with the increase of frequency. The ε'' of CoZnO@BPC-21 is the maximum, and the increase of ε'' leads to the increase of dielectric loss tangent ($tan\delta_e$) in Fig. 4c. The fluctuation of the dielectric loss peak is due to the multiple dielectric loss mechanisms caused by the hierarchical structure of the components and the complex chemical states. The increases of ε', ε'' and $tan\delta_e = {}^{\varepsilon''}/_{\varepsilon'}$ of CoZnO@BPC indicate that the dielectric loss capability of the composite is significantly enhanced by the attachment of MOF-derived metal or metal oxide nanoparticles, and the fluffy the pore channels of biomass carbon in the high frequency range.

In general, when the compositions undergo polarization relaxation, the values of ε' and ε'' can be plotted to form a semicircle on the Cole-Cole curve. More Cole-Cole semicircles indicate a stronger polarization relaxation process in the attenuation of EMW. This process is usually calculated by using the Debye relaxation equation [28]:

$$\left(\varepsilon' - \frac{\varepsilon_s + \varepsilon_\infty}{2}\right)^2 + \left(\varepsilon''\right)^2 = \left(\frac{\varepsilon_s - \varepsilon_\infty}{2}\right)^2 \quad (1)$$

where ε_S is the electrostatic constant, ε_∞ is the dielectric constant of infinite frequency. As seen in Fig. S3 (Supporting information), CoZnO@BPC-21 has larger and more semicircles in the ε''-ε' plots at 2-18 GHz, indicating the increase of Co particles enhance Debye dipole relaxation inside BPC under external electric fields.

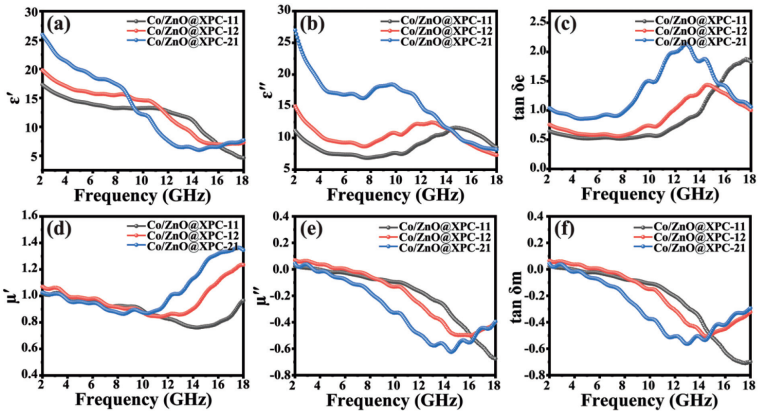

Fig. 4. Electromagnetic parameters of CoZnO/BPC composites with 20 wt% filling (a) real part of complex permittivity, (b) imaginary part of complex permittivity, (c) tangent of dielectric loss, (d) real part of complex permeability, (e) imaginary part of complex permeability, (f) tangent of magnetic loss.

These dipole relaxation processes are due to surface or interface polarization relaxation and displacement polarization, which result from the partially graphitized carbon containing defects and oxygen-containing groups as well as in more Co/C heterojunction nanostructures and fluffy carbon nanotubes. Besides, the imaginary part of the dielectric constant represents the decay capacity of the energy. As the frequency increases, the imaginary part of the complex dielectric constant decreases first and then increases to reach the peak. The dielectric constant of the sample showed a decreasing trend, indicating that the conductive loss played a leading role. The increasing trend of dielectric constant indicates that conductive loss is not the dominant role, and polarization relaxation occurs. In our samples, Due to the low content of Co and Zn, the μ' values of all samples are around 1 and the μ'' values are around 0 in Figs. 4d-f, indicating that the magnetic properties are weak. In view of the value μ'' reflects the magnetic loss capacity of the sample, and the magnetic loss capacity of the sample is basically similar. As the frequency rises, the fluctuation of μ'' value is evident at both low and high frequencies, with the fluctuation of low frequency mainly caused by natural resonance and the fluctuation of high frequency mainly caused by exchange resonance. The μ'' curve of the sample presents a negative value in the high-frequency region, which is due to the induced magnetic field generated by the material under the action of alternating electric field, and the magnetic energy radiates electromagnetic waves, resulting in a negative value of μ''. The trend of the tangent $tan\delta_m = \mu''/\mu'$ value of the magnetic loss is almost consistent with the trend of the virtual part μ'' of the complex permeability, which indicates that the magnetic loss of the composition is mainly determined by μ''. Considering that the filling amount is only 20%, and the amount of ZIF-8 and ZIF-67 particles coated to BPCs, the low μ'' and $tan\delta_m$ values of the compositions can be due to the low content of magnetic Co/C and ZnO/C particles in the sample.

Generally speaking, the magnetic loss of EMW absorber mainly includes hysteresis, domain wall resonance, eddy current resonance, and so on. Hysteresis stems are from the lag deflection of the magnetic moment with the alternating magnetic field. Domain wall resonances occur only in the low frequency range < 2 GHz. Eddy current loss and natural resonance is displayed $\mu''(\mu')^{-2}$ $(f)^{-1}$. Fig. S3b (Supporting information) shows the $\mu''(\mu')^{-2}$ $(f)^{-1}$ curve result for CoZnO@BPC. The fluctuation of $\mu''(\mu')^{-2}$ $(f)^{-1}$ of all compositions indicates that eddy current loss is not dominant, and magnetic loss is mainly from natural resonance and exchange resonance.

The reflection loss (RL) value, matched thickness and effective absorption bandwidth (EAB) are three most important factors for evaluating the EMW absorption performance. According to the transmission line theory, RL curves of CoZnO@BPC composites were investigated from the measured ε_r and μ_r at 2-18 GHz with the following equations [29]:

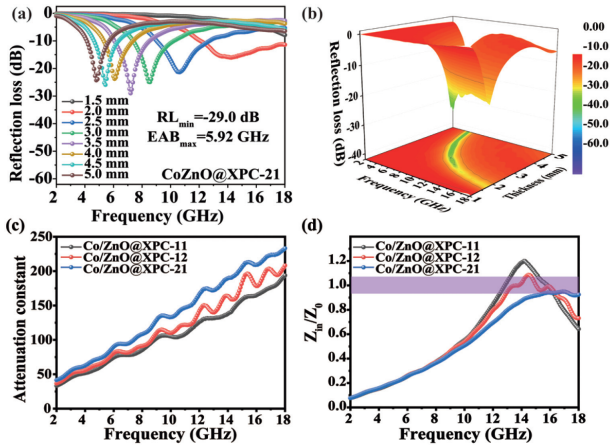

Fig. 5. CoZnO@BPC-21 for a thickness of 2.0 mm with (a, b) frequency dependence of RL, (c) overall attenuation constant diagram, (d) impedance matching.

$$Z_{in} = \sqrt{\frac{\mu_r}{\varepsilon_r}} tanh\left[j\left(\frac{2\Pi fd}{c}\right)\sqrt{\mu_r \varepsilon_r}\right] \quad (2)$$

$$RL = 20\log\left|\frac{Z_{in}-1}{Z_{in}+1}\right| \quad (3)$$

where Z_{in} represents the input impedance of metal-based layer, f is the frequency, d is the thickness of the absorber, c is the velocity of EMW, respectively. RL ≤ -10 dB is called effective EMW absorption.

The frequency-dependent RL of CoZnO@BPC composites with a filling amount of 20 wt% in the range of 2-18 GHz are showed in Figs. 5a-c and Fig. S4 (Supporting information). the RL_{min} value of CoZnO@BPC-11 reaches −50.2 dB although the EAB is only 4.0 GHz. However, the RL_{min} values of CoZnO@BPC-12 and CoZnO@BPC-21 are −44.5 dB and -29.0 dB, and the EAB is only 4.16 GHz and 5.92 GHz. Although CoZnO@BPC-21 has poor absorbing ability and weak RL value, its EAB is the widest, reaching 5.92 GHz. These can be easily found that the mass ratio of Zn^{2+} and Co^{2+} ions are vital for the absorption performance of the prepared samples. In addition, it is worth noting that with increasing of the thickness, the RL_{min}

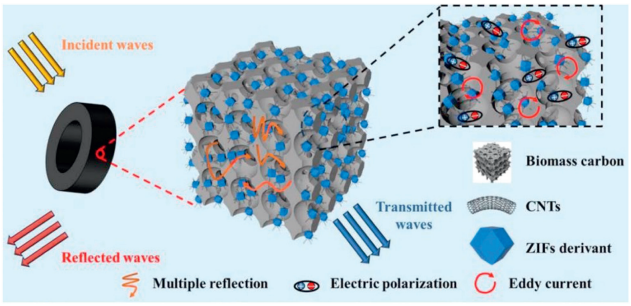

Fig. 6. EMW absorption mechanism diagram of CoZnO@XPC composite materials.

Table 1
EMW absorption properties derived from biomass composites.

Sample	Filler loading (wt%)	Thickness (mm)	RL_{min} (dB)	EAB (GHz)	Ref.
CoZnO@BPC-11	20	1.7	−50.2	4.0	This work
CoZnO@BPC-21	20	3.5	−29.0	5.92	This work
Ni $(OH)_2$/AC	50	5.5	−23.9	2.1	[31]
BC/FeCo	30	3	−40.1	4.7	[32]
PC@$NiFe_2O_4$	30	2.5	−50.8	4.9	[33]
$Ni_{0.5}Co_{0.5}Fe_2O_4$/BC	20	3	−41.6	4.3	[34]
Ni/C porous fibers	33	2.0	−43.0	4.9	[35]
HPC/Co-800	30	2.8	−52.6	5.44	[36]

peaks of all samples gradually move towards the low frequency region.

Attenuation constant (α) and impedance matching ($|Z_{in}/Z_0|$) are two most important coefficients to evaluate the EMW performance. α indicates the EMW attenuation ability of compositions, the larger α value, the stronger the EMW attenuation [30]. In addtion, if the value of $|Z_{in}/Z_0|$ is equal to 1, suggesting all the EMW enter into the material. As show Figs. 5c and d, the α of CoZnO@BPC-21 is greater than the others, the $|Z_{in}/Z_0|$ values of CoZnO@BPC-12 is closer to 1 in the range of 12-18 GHz. The $|Z_{in}/Z_0|$ values of CoZnO@BPC-11 and CoZnO@BPC-12 differ greatly from 1, which can be explain why CoZnO@BPC-21 has better EMW absorption capacity.

The CoZnO@BPC EMW mechanism of the composite are deduced in Fig. 6. First, the synergistic effect of the magnetic loss of ZIFs and the dielectric loss of BPCs provides better impedance matching conditions, resulting in more EMW being transmitted to the composites. Secondly, the cellular structure also enhances the ability of electromagnetic energy dissipation. On the one hand, the three-dimensional intercommunicating porous carbon skeleton structure causes multiple scattering of incident EMW, which is attributed to extending the propagation path of absorbed EMW and enhancing the energy dissipation ability of EMW. On the other hand, Co/carbon, ZnO/carbon, carbon/paraffin and C/air form rich heterogeneous interfaces, resulting in increased interface and multi-polarization effect, which will produce stronger dielectric losses. Finally, the conduction loss and dipole polarization are caused by oxygen-containing functional groups and N doping in the porous carbon derived from the shell also contribute to the dielectric loss.

The electromagnetic absorption properties of composites derived from biomass are shown in Table 1 [31–36]. Obviously, CoZnO@BPC has good electromagnetic absorption properties compared with related materials. Therefore, reasonably designed CoZnO@XPC composites have broad application prospects in the field of electromagnetic absorption.

In summary, biomass Carbon/ZIF composites derived from XSBS for EMW absorption were successfully prepared by simple pyrolysis. The effect of mass ratio of Zn to Co in magnetic metal ZIF on EMW absorption performance was investigated. The prepared CoZnO@BPC has good impedance matching property, strong dielectric loss capability, and relative lightweight, contributing to a high-performace EMW absorption. The results showed that when the filling amount is 20 wt% and the mass ratio of Zn to Co is 1:1, the RL_{min} and EAB of CoZnO@BPC-11 at a matching thickness of 1.7 mm can reach −51.2 dB and 4.0 GHz respectively. When the mass ratio of Zn to Co is 2:1, the minimum reflection loss of CoZnO@BPC-21 at 3.5 mm is −29.0 dB, and the EAB can be up to 5.92 GHz. The introduction of metal magnetic particles makes the biomass carbon surface form a rich heterogeneous interface, resulting in more interface polarization and dipole polarization, and stronger dielectric loss in the end. This work provides a new idea for the further effective utilization of biowaste and the in-depth exploration of EMW absorption mechanism.

Declaration of competing interest

The authors declare that they have no known competing financial interests or personal relationships that could have appeared to influence the work reported in this paper.

CRediT authorship contribution statement

Xuexia Lin: Investigation, Methodology, Data curation, Writing – original draft, Writing – review & editing. **Yihui Zhou:** Investigation, Methodology, Data curation, Writing – original draft, Writing – review & editing. **Jiafu Hong:** Investigation, Methodology, Data curation, Writing – original draft, Writing – review & editing. **Xiaofeng Wei:** Investigation, Methodology, Writing – review & editing. **Bin Liu:** Investigation, Methodology, Writing – review & editing. **Chong-Chen Wang:** Investigation, Methodology, Writing – review & editing.

Acknowledgment

This work was financially supported by Natural Science Foundation of Fujian Province (Nos. 2021T3024, 2021H0017 and 2022H0016).

Supplementary materials

Supplementary material associated with this article can be found, in the online version, at doi:10.1016/j.cclet.2024.109835.

References

[1] X. He, H. Peng, Z. Xiong, et al., Carbon 198 (2022) 195–206.
[2] X. Wen, C. Li, H. Liu, et al., J. Mater. Sci. Technol. 170 (2023) 1–10.
[3] R. Guo, D. Su, F. Chen, et al., ACS Appl. Mater. Interfaces 14 (2022) 3084–3094.
[4] X. Huang, Y. Wang, Z. Lou, et al., Carbon 209 (2023) 118005.
[5] X. Lu, D. Zhu, X. Li, et al., Adv. Compos. Hybrid. Mater. 4 (2021) 946–956.
[6] S. Dong, P. Hu, X. Li, et al., Chem. Eng. J. 398 (2020) 125588.
[7] Z. Yu, R. Zhou, M. Ma, et al., J. Mater. Sci. Technol. 114 (2022) 206–214.
[8] Z. Tang, L. Xu, C. Xie, et al., Nat. Commun. 14 (2023) 5951.
[9] X. Zhang, B. Li, J. Xu, et al., Adv. Funct. Mater. 33 (2023) 2210456.
[10] H. Zhao, Y. Cheng, H. Lv, et al., ACS Sustainable Chem. Eng. 6 (2018) 15850–15857.
[11] X. Sun, M. Yang, S. Yang, et al., Small 15 (2019) 1902974.
[12] X. Xie, Y. Wang, X. Sun, et al., J. Mater. Sci. Technol. 133 (2023) 1–11.
[13] R. Zhang, J. Qiao, X. Zhang, et al., Mater. Chem. Phys. 289 (2022) 126437.
[14] H. Yan, B. Fu, S. Xuan, T. Qin, X. Yao, Compos. Struct. 321 (2023) 117280.
[15] X. Lin, J. Hong, C.C. Wang, M. Su, S. F, J. Mater. Chem. A 11 (2023) 17737–17745.
[16] W. Zhang, X. Jiang, X. Wang, et al., Angew Chem. Int. Ed. 56 (2017) 8435–8440.
[17] H. Chen, K. Shen, J. Chen, X. Chen, Y. Li, J. Mater. Chem. A 5 (2017) 9937–9945.
[18] L. Hu, P. Zhang, Y. Sun, S. Bao, Q. Chen, ChemPhysChem 14 (2013) 3953–3959.
[19] Y.Z. Chen, C. Wang, Z.Y. Wu, et al., Adv. Mater. 27 (2015) 5010–5016.
[20] D. Zeng, Y. Yang, F. Yang, et al., Nanoscale 9 (2017) 11851–11857.
[21] R. Qiang, Y. Du, D. Chen, et al., J. Alloy. Compd. 681 (2016) 384–393.
[22] Q. Liao, M. He, Y. Zhou, et al., Langmuir 34 (2018) 15854–15863.
[23] L. Qiao, C. Wang, X.S. Zhao, ACS Appl. Energy Mater. 4 (2021) 7012–7019.
[24] L. Yang, X. Zhou, Z. Jia, et al., Carbon 167 (2020) 843–851.

[25] H. Yan, X. Xue, Y. Fu, X. Wu, J. Dong, Ceram. Int. 46 (2020) 9729–9733.
[26] J. Xu, J. Wu, L. Luo, et al., J. Power Sources 274 (2015) 816–822.
[27] Y. Zhang, X. Liu, Z. Guo, et al., J. Mater. Sci. Technol. 176 (2024) 167–175.
[28] F. Zhang, S. Yin, Y. Chen, et al., Chem. Eng. J. 433 (2022) 133586.
[29] J. Tao, Z. Jiao, L. Xu, et al., Carbon. 184 (2021) 571–582.
[30] G. Chen, L. Zhang, B. Luo, H. Wu, J. Colloid Interf. Sci. 607 (2022) 24–33.
[31] H. Guan, H. Wang, Y. Zhang, et al., Appl. Surf. Sci. 447 (2018) 261–268.
[32] X. Pang, L. Ye, X. Li, et al., J. Alloy Compd. 888 (2021) 161510.
[33] Y. Wang, X. Gao, H. Zhou, et al., Powder Technol. 345 (2019) 370–378.
[34] J. Sun, J. Chen, H. Ge, et al., Compos. Part A: Appl. S. 156 (2022) 106850.
[35] W. Li, F. Guo, X. Wei, Y. Du, Y. Chen, RSC Adv. 10 (2020) 36644–36653.
[36] T. Liu, N. Liu, L. Gai, et al., Micropor. Mesopor. Mat. 302 (2020) 110210.